Solid State Communications 218 (2015) 10–13

Contents lists available at ScienceDirect

Solid State Communications

journal homepage: www.elsevier.com/locate/ssc

Dielectric and piezoelectric properties of $BiFeO_3$ from molecular dynamics simulations

M. Graf, M. Sepliarsky *, R. Machado, M.G. Stachiotti

Instituto de Física Rosario, Universidad Nacional de Rosario, 27 de Febrero 210 Bis, 2000 Rosario, Argentina

ARTICLE INFO

Article history:
Received 28 May 2015
Accepted 3 June 2015
Communicated by A.H. MacDonald
Available online 12 June 2015

Keywords:
A. $BiFeO_3$
C. Atomistic simulations
D. Piezoelectric properties

ABSTRACT

A first-principles based atomistic scheme is used to investigate the dielectric and piezoelectric properties of $BiFeO_3$. The atomistic model fitted from first-principles calculations reproduces very well the structural and polar properties of the material at finite temperature, predicting a direct transition from a low-temperature *R3c* ferroelectric phase to a *Pbnm* orthorhombic phase in agreement with experiments. We use this theoretical approach to calculate intrinsic single crystal properties, which are difficult to obtain from experiments due to decomposition and leakage problems. The whole set of dielectric and piezoelectric coefficients for $BiFeO_3$ is computed as a function of temperature, together with the orientation dependence of the longitudinal coefficient d^*_{33}.

© 2015 Elsevier Ltd. All rights reserved.

1. Introduction

The perovskite $BiFeO_3$ (BFO) has become the prototypical single compound to understand multiferroic behavior. The interest in BFO is mainly driven by the coexistence of ferroelectric and antiferromagnetic ordering at room temperature, and it is expected to have a wide range of novel applications [1–7]. Beside the interest in its magnetoelectric properties, BFO is attracting a lot of attention as a lead-free ferroelectric compound for eco-friendly devices [8,9] since it posses large intrinsic polarization and high Curie temperature. Even more, the discovery of a morphotropic phase boundary in strained epitaxial films as well as in BFO-based solid solutions makes the system suitable for high-performance piezoelectric applications [10–13].

Extensive experimental and theoretical studies have been devoted to characterize the structural and physical properties of the compound. Much progress has been made, although controversies still remaining. The room-temperature phase of BFO is classed as rhombohedral (point group *R3c*) with two formula units per unit cell, a ferroelectric polarization along the [111] pseudocubic direction [14] and an antiphase tilting of oxygen octahedral rotations. At approximately 825 °C there is a first-order transition to an orthorhombic phase of *Pbnm*-symmetry (formally *Pnma*) with four formula units per unit cell [15]. The transition is accompanied by a marked volume contraction. Nevertheless, the possibility of an intermediate bridging region between the low and high temperatures phases has been suggested [16]. The polar nature of the high-temperature phase is also not settled. While this phase has been seen as paraelectric in experiments, signals related to an antiferroelectric (AFE) order have been suggested [17–20].

The determination of the intrinsic dielectric and piezoelectric properties of BFO are also controversial [21] and references therein. Experimental studies are carried out mainly on polycrystalline systems and rarely on single crystals due to the lack of crystals of sufficiently good quality. To make matters worse, obtaining single-phase perovskite materials free of impurity phases, such as $Bi_2Fe_4O_9$ and $Bi_{25}FeO_{39}$, is very difficult. Another important shortcoming is the high electrical conductivity, and a complete experimental characterization at high temperature is cumbersome due to leakage problems. In addition, the unfortunate combination of the high electrical conductivity and the high coercive field, leads to difficulties in studying piezoelectricity. Given this controversial experimental background, the determination of the intrinsic properties of BFO using a reliable theoretical approach is highly desirable. In this paper we report the dielectric and piezoelectric properties of BFO using a first-principles based atomistic model, which has the advantage of accurately predicting the temperature-driven phase transition sequence of the material [20].

2. Computational method

First-principles methods are a very powerful tool for investigating the properties of ferroelectric perovskites theoretically [22]. However, these methods are essentially restricted to the study of the zero-temperature properties using rather small number of atoms. It is obviously of primary importance to predict finite-temperature

* Corresponding author. Tel.: +54 341 4853200.
E-mail address: sepliarsky@ifir-conicet.gov.ar (M. Sepliarsky).

http://dx.doi.org/10.1016/j.ssc.2015.06.002
0038-1098/© 2015 Elsevier Ltd. All rights reserved.

properties. The most widespread approaches to this problem are the effective Hamiltonians and the atomistic shell models. Atomic level simulations using shell models have been extensively used to study ferroelectric oxides [23–24] and their piezoelectric properties [25–26]. In this approach, atoms are thought to consist of an ion core coupled to an "electronic" shell in order to include its electronic polarization. The core–shell coupling is described through an anharmonic spring described as $V(\omega)=1/2k_2\omega^2+1/24\ k_4\ \omega^4$, where ω is the core–shell displacement. Besides the "intra-atomic" core–shell coupling, the model includes electrostatic interactions among cores and shells of different atoms, and short-range interactions between shells described by a Rydberg potential, $V(r)=(a+Br)\ exp(-r/\rho)$. All these material-specific parameters are determined by first-principles calculations. See Ref. [20] for details about the parametrization of the model for BFO. In this work we apply the interatomic potentials developed for BFO to determine the dielectric and piezoelectric properties of this material at finite temperature. For that purpose, Molecular dynamics (MD) simulations were carried out using the DL-POLY code [27] within a constant stress and temperature (N, σ, T) ensemble. In this way, the size and shape of the simulation cell are dynamically adjusted in order to obtain the desired average pressure. A supercell size of $12\times12\times12$ 5-atom unit cells (8640 atoms) was used with periodic boundary conditions. The runs were made at temperature intervals of 50 K, and with a time step of 0.4 fs. Each MD run consists of at least 40,000 time steps for data collection after 20,000 time steps for thermalization. The dielectric and piezoelectric coefficients were computed at selected temperatures by the changes produced by applied electric fields in the polarization and in strains components, respectively.

3. Results and discussion

We highlight first the main achievements of our theoretical scheme for the description of the temperature-driven phase transition in BFO. Fig. 1 displays the temperature evolution of the lattice parameters along pseudo-cubic directions obtained from MD simulations. Clearly, a phase transition with a strong first-order character takes place. The lattice parameters, that increase with temperature due to thermal expansion, display a marked reduction at $T_C=830$ °C, in agreement with experiments. The volume contraction is ~1.98%, which is close to the experimental value of 1.56% [28].

The low-temperature phase has *R3c* symmetry. It is characterized by identical values of cell parameters and a polarization pointing along the [111] direction. The order parameters related with oxygen tilts display the anti-phase octahedral tilting pattern characteristic of the *R3c* symmetry. At room-temperature, for example, the model has spontaneous polarization $P=77\ \mu C\ cm^{-2}$ and a tilting angle around the [111] axis is 13.8°, which are comparable with the values reported in experiments [15,29]. The lattice constants are in reasonable agreement with experiments, although the cell parameters are underestimated as a result of the *LDA* input data used for the fitting.

Above T_C the macroscopic polarization vanishes and the system adopts *Pbnm* symmetry, in agreement with experiments [3]. The high-temperature *Pbnm* phase is characterized by two sublattices with opposite polarizations, generated by Bi off-center displacements. This feature supports the antiferroelectric nature of the *Pbnm* phase [20]. The oxygen octahedron tilting becomes in-phase along z while it remains out-of-phase along the other two directions. The insets of Fig. 1 show, schematically, the main differences between the low- and high-temperature phases. We thus conclude that the atomistic model, entirely developed from first-principles calculations (i.e. no explicit experimental data has been used as input), describes the *R3c*–*Pbnm* phase transition in good agreement with experiments.

One advantage of our theoretical approach is the possibility to calculate single crystal properties, which are important to determine the anisotropy of the material. Then we investigate the intrinsic dielectric and piezoelectric properties of BFO through the calculation of the corresponding coefficients. Fig. 2 shows the dielectric susceptibilities along crystallographic directions as a function of temperature. For the *R3c* structure we choose the polar direction along the z-axis, in such a way that the [111] axes of the cubic phase correspond to the direction $X_3=[001]_R=[111]_C$. The other two axis are $X_1=[100]_R=[1\text{–}10]_C$ and $X_2=[010]_R=[11\text{–}2]_C$. The coordinate system used for the orthorhombic *Pbnm* phase was $X_1=[100]_O=[110]_C$, $X_2=[010]_O=[-110]_C$ and $X_3=[001]_O=[001]_C$. At room temperature the dielectric coefficients of the *R3c* phase are $\varepsilon_{33}=23$ and $\varepsilon_{11}=\varepsilon_{22}=36$. These values are in concordance with the rather small value of $\varepsilon\sim30$ [30,31] measured in ceramics for the GHz dielectric permittivity. We note that extremely high values of ε were reported in the Hz-to-MHz frequency range, both in ceramics [30] and single crystals [32]. This is due however to the contribution of extrinsic factors, like domain wall motions and electrical conductivity.

The small values obtained for ε_{ij} coefficients can be understood from the fact that transition temperature in BFO is at 830 °C and the ferroelectric polarization is saturated at room temperature. In fact, Fig. 2 shows that both, ε_{11} and ε_{33} increases slightly with temperature up to ~630 °C. From there, the thermal instability of ε_{33} increases due to the proximity with the rhombohedral–orthorhombic transition

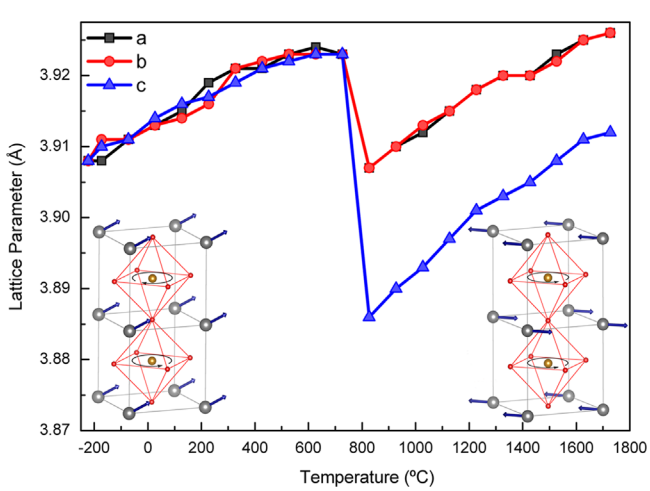

Fig. 1. (color online) Thermal evolution of lattice parameters of $BiFeO_3$ resulting from the MD simulations. The insets show schematically the main differences between the *R3c* and *Pbnm* phases: Bi off-center displacements and oxygen octahedron tilting.

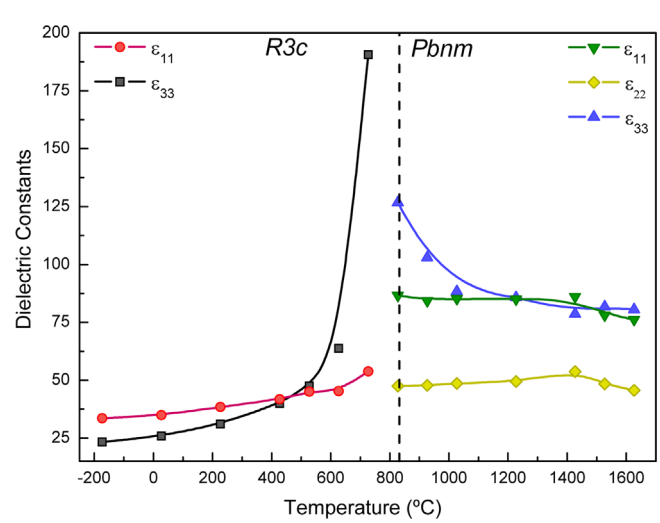

Fig. 2. (color online) Temperature dependence of the dielectric permittivity coefficients along the crystallographic directions determined from MD simulations.

where this coefficient displays a sharp peak reaching the value of 200. All these features are in concordance with the fact that the transition has a strong first-order character and there is little phonon softening. In this way, the dielectric constant obtained from the Lyddane–Sachs–Teller dielectric relationship can be expected to be low.

The thermal evolution of the piezoelectric constants obtained from MD simulations is shown in Fig. 3. The data are plotted below T_c because the non-polar *Pbnm* phase is not piezoelectric. From symmetry considerations, there are four independent piezoelectric coefficients for the ferroelectric *R3c* phase: the longitudinal d_{33} and d_{22}, the transverse d_{31}, and the shear component d_{15}. We observe that the room-temperature piezoelectric coefficients are rather small compared to typical perovskite ferroelectrics, such as $BaTiO_3$, $PbZr_xTi_{1-x}O_3$. The coefficients present also another unusual characteristic, they are all positive. We note that while d_{31} is positive in BFO, this coefficient is negative in the isostructural materials $LiTaO_3$ and $LiNbO_3$ [33]. In all cases, however, the values of d_{31} are very small. What is important to note is that d_{33} is the highest coefficient over the entire temperature range. This coefficient increases with temperature similarly to what is observed in typical ABO_3 perovskites below their Curie point. At room temperature d_{33} is small ($\sim$18 pm/V), in concordance with experimental values. We note that there is a very broad range of reported values in ceramics, from 4 pm/V to 60 pm/V [34–37]. The problem is the high electrical conductivity of the samples which prevents the application of a high electric field for an efficient poling. The other piezoelectric coefficients obtained from the MD simulations are even much smaller and display a higher thermal stability.

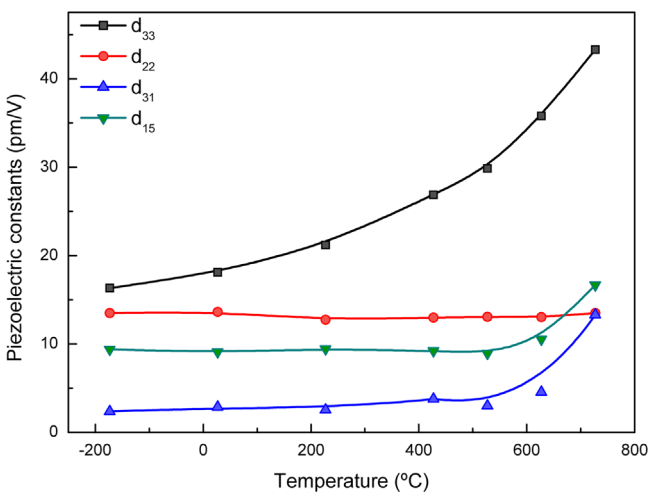

Fig. 3. (color online) Piezoelectric coefficients as a function of temperature obtained through MD simulations.

Now that the piezoelectric coefficients d_{ij} of a monodomain single crystal are known, we can calculate the piezoelectric properties of BFO along a general nonpolar direction d^*_{ij} via simple coordinate transforms [33,38]. For instance, the calculation of the longitudinal piezoelectric coefficient d^*_{33} as a function of orientation reveals much about the piezoelectric anisotropy of a material. So we compute d^*_{33} for the *R3c* phase of BFO as:

$$d^*_{33}(\theta,\Phi,\Psi) = \cos\theta\ \sin^2\theta\,(d_{15}+d_{31}) + \cos^3\theta\ d_{33} + \sin^3\theta\ \cos\Phi\left(3\sin^2\Phi - \cos^2\Phi\right) d_{22}$$

where θ, Φ and Ψ are the Euler angles. Fig. 4(a) shows a polar plot of the room temperature d^*_{33} coefficient as a function of orientation with respect to the orthogonal axes of the monodomain rhombohedral crystal. The distance from the origin to the 3D surface

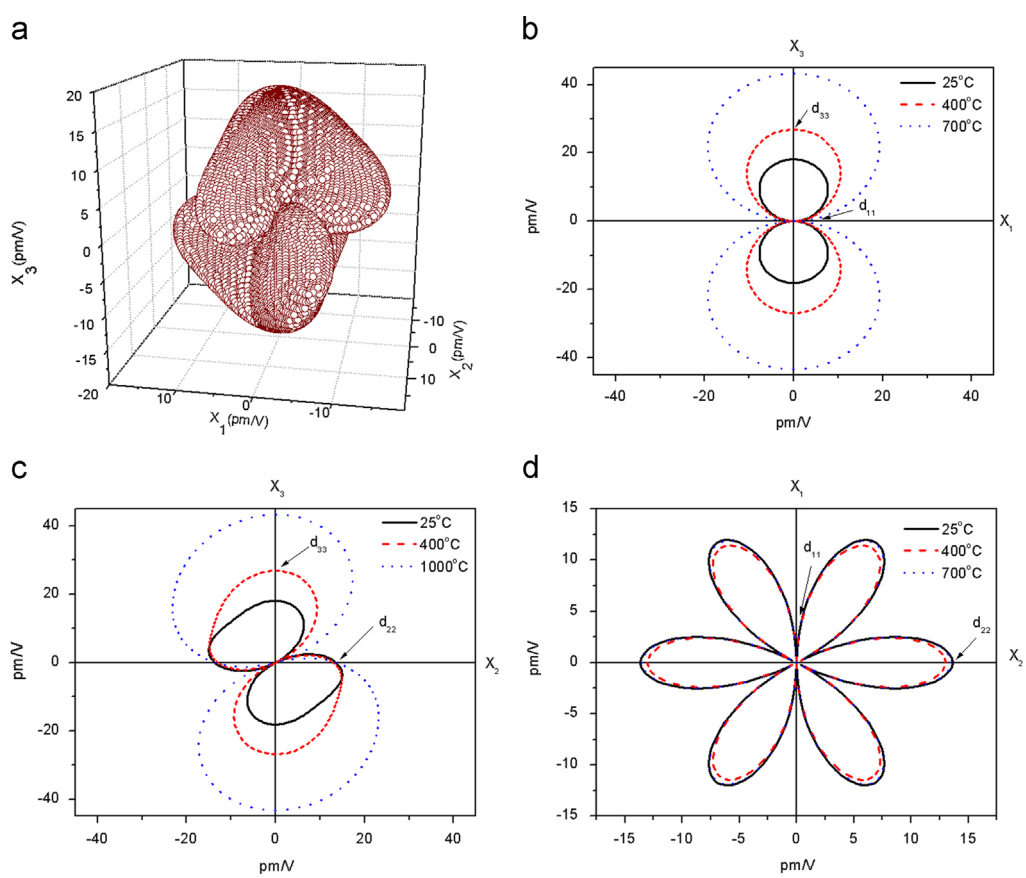

Fig. 4. (color online) (a) Orientation dependence of the piezoelectric coefficient d^*_{33} in the *R3c* phase of BFO at room temperature. (b–d) The piezoelectric coefficient d^*_{33} at various temperatures for three different cutting planes of the 3D surface.

in a certain direction gives a measure of d^*_{33} in that direction. Figs. 4(b–d) display the piezoelectric d^*_{33} coefficients at various temperatures using three cutting planes of the 3D surface. Immediately apparent is that the highest value of d^*_{33} is along the polar direction. It is well known in ferroelectrics that the maximum of d^*_{33} does not lie always along the polar direction, and that the enhancement out of that direction can occur due to a phase transition at which the polarization changes its direction. In this way the piezoelectric anisotropy increases close to ferroelectric–ferroelectric phase transitions. Clearly this is not the case in BFO where the transition is from a ferroelectric to a non-polar phase. In this regards, BFO resembles the case of $PbTiO_3$. $PbTiO_3$ has a phase transition from a ferroelectric to a non-polar cubic phase, and the highest value of d^*_{33} is found along the polar direction [33]. The piezoelectric anisotropy, defined as the ratio of shear and longitudinal coefficients d_{15}/d_{33}, is around 0.7 in $PbTiO_3$ [33] and 0.16 in BFO. It is interesting to point out that a strong increase of the piezoelectric anisotropy can be expected in BFO if the material is under strain. This is due to the formation of a morphotropic phase boundary between the *R3C* and a tetragonal ferroelectric phase [10].

4. Conclusions

The dielectric and piezoelectric coefficient tensors and the orientation dependence of longitudinal piezoelectric coefficient d^*_{33} for $BiFeO_3$ were computed at different temperatures using a first-principles based atomistic approach. The rather small values obtained for the room-temperature dielectric coefficients are in concordance with the value measured for the GHz dielectric permittivity, while the much higher values reported in the Hz-to-MHz frequency range are due to extrinsic contributions and/or a high electrical conductivity of the samples. The piezoelectric coefficients are also rather small compared to typical ferroelectric perovskites. The maximum of d^*_{33} lies along the polar direction of the *R3c* phase in the entire temperature range and the material displays a very low piezoelectric anisotropy. We hope that the determination of the intrinsic dielectric and piezoelectric coefficients for $BiFeO_3$ contribute to better understand the properties of this fascinating material.

Acknowledgments

We acknowledge computing time at the CCT-Rosario Computational Center. The work was sponsored by Consejo Nacional de Investigaciones Científicas y Tecnológicas (CONICET), Agencia Nacional de Promoción Científica y Tecnológica (ANPCyT) and Universidad Nacional de Rosario. MGS thanks support from Consejo de Investigaciones de la Universidad Nacional de Rosario (CIUNR).

References

[1] W. Eerenstein, N.D. Mathur, J.F. Scott, Nature 442 (2006) 759.
[2] J. Neaton, C. Ederer, U. Waghmare, N. Spaldin, K. Rabe, Phys. Rev. B 71 (2005) 1.
[3] G. Catalan, J.F. Scott, Adv. Mater. 21 (2009) 2463.
[4] Y.E. Roginskaya, et al., Sov. Phys. JETP 23 (1966) 47.
[5] W. Kaczmarek, Z. Pajak, Solid State Commun. 17 (1975) 807.
[6] G.A. Smolenskii, V.M. Yudin, Sov. Phys. Solid State 6 (1965) 2936.
[7] A.P. Pyatakov, A.K. Zvezdin, Phys.-Uspekhi 55 (2012) 557.
[8] R. Ramesh, N. Spaldin, Nat. Mater. 6 (2007) 21.
[9] T. Rojac, A. Bencan, G. Drazic, M. Kosec, D. Damjanovic, J. Appl. Phys. 112 (2012) 064114.
[10] R.J. Zeches, M.D. Rossell, J.X. Zhang, A.J. Hatt, Q. He, C.-H. Yang, A. Kumar, C.H. Wang, A. Melville, C. Adamo, G. Sheng, Y.-H. Chu, J.F. Ihlefeld, R. Erni, C. Ederer, V. Gopalan, L.Q. Chen, D.G. Schlom, N.A. Spaldin, L.W. Martin, R. Ramesh, Science 326 (2009) 977.
[11] S. Fujino, M. Murakami, V. Anbusathaiah, S.-H. Lim, V. Nagarajan, C.J. Fennie, M. Wuttig, L. Salamanca-Riba, I. Takeuchi, Appl. Phys. Lett. 92 (2008) 202904.
[12] D. Kan, L. Pálová, V. Anbusathaiah, C.J. Cheng, S. Fujino, V. Nagarajan, K.M. Rabe, I. Takeuchi, Adv. Funct. Mater. 20 (2010) 1108.
[13] A.Y. Borisevich, E.A. Eliseev, A.N. Morozovska, C.-J. Cheng, J.-Y. Lin, Y.H. Chu, D. Kan, I. Takeuchi, V. Nagarajan, S.V. Kalinin, Nat. Commun. 3 (2012) 775.
[14] F. Kubel, H. Schmid, Acta Crystallogr. Sect. B: Struct. Sci. 46 (1990) 698.
[15] D.C. Arnold, K.S. Knight, F.D. Morrison, P. Lightfoot, Phys. Rev. Lett. 102 (2009) 027602.
[16] S. Prosandeev, D. Wang, W. Ren, J. Íñiguez, L. Bellaiche, Adv. Funct. Mater. 23 (2013) 234.
[17] I.A. Kornev, S. Lisenkov, R. Haumont, B. Dkhil, L. Bellaiche, Phys. Rev. Lett. 99 (2007) 227602.
[18] O. Diéguez, O. González-Vázquez, J. Wojdeł, J. Íñiguez, Phys. Rev. B 83 (2011) 094105.
[19] Y.-M. Kim, A. Kumar, A. Hatt, A.N. Morozovska, A. Tselev, M.D. Biegalski, I. Ivanov, E.A. Eliseev, S.J. Pennycook, J.M. Rondinelli, S.V. Kalinin, A.Y. Borisevich, Adv. Mater. 25 (2013) 2497.
[20] M. Graf, M. Sepliarsky, S Tinte, M.G. Stachiotti, Phys. Rev. B 90 (2014) 184108.
[21] T. Rojac, A. Bencan, B. Malic, G. Tutuncu, J.L. Jones, J.E. Daniels, D. Damjanvic, J. Am. Ceram. Soc. 97 (2014) 1993.
[22] L. Belleiche, Curr. Opin. Solid State Mater. Sci. 6 (2002) 19.
[23] M. Sepliarsky, A. Asthagiri, S.R. Phillpot, M.G. Stachiotti, R.L. Migoni, Curr. Opin. Solid State Mater. Sci. 9 (2005) 107.
[24] R. Machado, M. Sepliarsky, M.G. Stachiotti, Appl. Phys. Lett. 93 (2008) 242901.
[25] R. Machado, M. Sepliarsky, M.G. Stachiotti, J. Mater. Sci. 45 (2010) 4912.
[26] R. Machado, M. Sepliarsky, M.G. Stachiotti, Appl. Phys. Lett. 103 (2013) 242901.
[27] I.T. Todorov, W. Smith, K. Trachenko, M.T. Dove, J. Mater. Chem. 16 (2006) 1911.
[28] D. Lebeugle, D. Colson, A. Forget, M. Viret, Appl. Phys. Lett. 91 (2007) 022907.
[29] A. Palewicz, R. Przeniosło, I. Sosnowska, A.W. Hewat, Acta Crystallogr. Sect. B: Struct. Sci. 63 (2007) 537.
[30] S. Kamba, D. Nuzhnyy, M. Savinov, J. Sebek, J. Petzelt, J. Prokleska, R. Hamont, J. Kreisel, Phys. Rev. B 75 (2007) 024403.
[31] W. Kaczmarek, Z. Pajak, M. Polomska, Solid State Commun. 17 (1975) 807.
[32] J. Lu, A. Gunther, F. Schrettle, F. Mayr, S. Krohns, P. Lunkenheimer, A. Pimenov, V.D. Travkin, A.A. Mukhin, A. Loidl, Eur. Phys. J. B 75 (2010) 451.
[33] M. Davis, M. Budimir, D. Damjanovic, N. Setter, J. Appl. Phys. 101 (2007) 054112.
[34] G.L. Yuan, S.W. Or, Y.P. Wang, Z.G. Liu, J.M. Liu, Solid State Commun. 138 (2006) 76.
[35] V.V. Shvartsman, W. Kleemann, R. Haumont, J. Kreisel, Appl. Phys. Lett. 90 (2007) 172115.
[36] Z. Dai, Y. Akishige, J. Phys. D: Appl. Phys. 43 (2010) 445403.
[37] Y. Yao, B. Ploss, C.L. Mak, K.H. Wong, Appl. Phys. A 99 (2010) 211.
[38] M. Davis, D. Damjanovic, D. Hayem, N. Setter, J. Appl. Phys. 98 (2005) 014102.